Graphical Abstract

Pillar[n]MaxQ Sensing Ensemble: Application to World Anti-Doping Agency Banned Substances

Leave this area blank for abstract info.

David King[a], Chun-Lin Deng,[a] and Lyle Isaacs [a,*]

[a] *Department of Chemistry and Biochemistry, University of Maryland, College Park, MD 20742 (USA)*

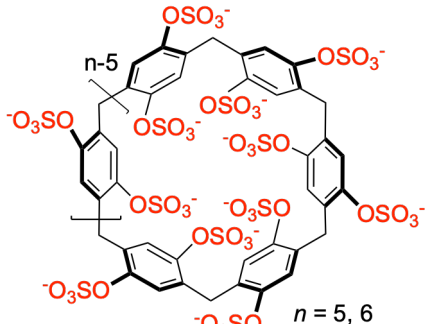

Tetrahedron
journal homepage: www.elsevier.com

Pillar[n]MaxQ Sensing Ensemble: Application to World Anti-Doping Agency Banned Substances

David King,[a] Chun-Lin Deng,[a] and Lyle Isaacs [b,*]

[a] *Department of Chemistry and Biochemistry, University of Maryland, College Park, MD 20742 (USA)*

ARTICLE INFO

Article history:
Received
Received in revised form
Accepted
Available online

Keywords:
Pillararene
Sensing ensemble
WADA banned substances
Host-Guest chemistry

ABSTRACT

The molecular recognition properties of two pillar[*n*]arene sulfates (P[5]AS and P[6]AS) toward a panel of world anti-doping agency banned substances (**1** – **11**) were investigated by a combination of isothermal titration calorimetry, ^{1}H NMR spectroscopy, and molecular modelling. Subsequently a sensing ensemble based on indicator displacement was created using the P[5]AS•lucigenin and P[6]AS •Hoechst 33258 complexes which allowed differentiation among the analytes with 90% accuracy. The assay was extended to allow the quantitation of pseudoephedrine in simulated urine samples with a limit of quantitation that is 30-fold below the WADA threshold.

1. Introduction.

Sports constitute a universal language that are enjoyed by people worldwide both at the professional level and at the amateur level. The economic impacts of professional sports are substantial whereas at the amateur level (e.g. Olympic games) considerations of national pride and rivalries play large motivating factors. Accordingly, it is imperative that measures are taken to ensure that athletes are competing fairly and not taking substances that give them an unfair advantage.[1] This has proven challenging to say the least with notable scandals including the use of steroids in Major League Baseball in the early 2000's that lead to Congressional hearings[2] and the state-sponsored doping of Russian athletes.[3] Most recently, in 2021 the International Olympic Committee announced that weightlifting was removed from the list of events for the 2028 Olympics with the press release naming the "historical incidence of doping" as a contributing factor.[4] The world anti-doping agency (WADA) develops and coordinates anti-doping rules across sports and countries and maintains a list of WADA-banned substances.

Currently, the most accurate and precise drug testing is performed using analytical techniques such as gas-chromatography,[5] and ultra high-performance liquid chromatography,[5b, 6] however, they are expensive and are not mobile. Advancements in light-based sensors and enzyme-linked immunoassays allow for the relatively quick detection of prohibited substances.[5a, 6-7] Within the realm of supramolecular chemistry, the use of indicator displacement assays (IDA)[7a, 8] have been effective at the detection and differentiation of numerous classes of compounds including steroids,[9] opioids,[10] and amphetamines[8, 11] in biologically relevant media. The creation of such indicator displacement assays relies on the ready availability of supramolecular hosts that both bind dyes and display either high selectivity or a broad based affinity profile toward suitable analytes to enable either lock-and-key or differential sensing approaches.[12] A variety of hosts including calixarenes, cyclodextrins, cyclophanes, cucurbiturils, and pillararenes have been used to construct chemical sensing systems.[7b, 8, 13] We have recently reported sulfated pillararenes (P[*n*]AS) as a new class of water soluble pillararenes that engage in high affinity interactions with a variety of hydrophobic (di)cations in aqueous solution (Figure 1).[14] For example, P[6]AS was shown to bind with nanomolar affinity toward post-translationally modified amino acids and peptides, drugs of abuse (opioid and non-opioid), and neuromuscular blocking agents.[14-15] In this paper, we investigate the binding of P[*n*]AS toward a panel of compounds that appear on the 2023 WADA Prohibited List[16] or are close structural analogues and the construction of a sensing assay for the WADA-banned substances based on indicator displacement using the P[5]AS•lucigenin and P[6]AS•Hoechst 33258 complexes.

* Corresponding author. Tel.: +1 301-405-1884; fax: +1 301-314-9121;
e-mail: LIsaacs@umd.edu

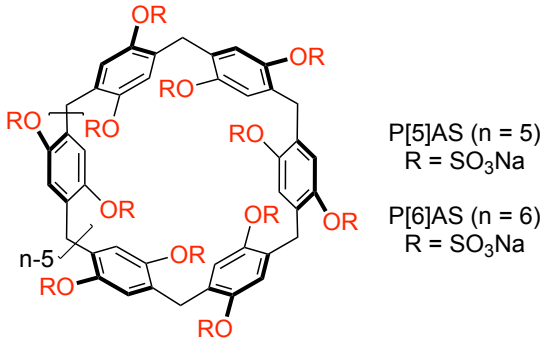

Fig. 1. Chemical structures of pillararenes used in this study.

2. Results and discussion.

This results and discussion section is organized as follows. First, we discuss the selection of the hosts, dyes, and WADA banned substances. Next, we present the thermodynamic parameters of P[*n*]AS•guest binding determined by isothermal titration calorimetry. Subsequently, we use ^{1}H NMR spectroscopy to determine binding induced changes in chemical shift and thereby glean information about P[*n*]AS•guest geometry. Finally, we use P[*n*]AS (n = 5, 6) along with the dyes lucigenin and Hoechst 33258 to identify the WADA banned substances and to quantify epinephrine and pseudoephedrine in simulated urine.

2.1. Selection of Host, WADA Banned Substances, and Dyes.

As discussed above, P[*n*]AS (Figure 1) display high binding affinity and high selectivity toward hydrophobic cations in aqueous solution[14] which make them attractive components of sensing ensembles for numerous analytes. From amongst the list of WADA banned substances,[16] we selected 13 compounds for this initial study including eight stimulants and four steroids (Figure 2). Given the preference of pillar[5]arenes for linear alkane derivatives[17] over cyclic compounds, we selected compounds **1** – **6** which to probe the influence of chain length and branching location on P[5]AS•guest binding. Compounds **2** – **4** and **6** were purchased and used as the racemic mixture, whereas **5** is a mixture of diastereomers. Conversely, P[6]AS is a more voluminous host which binds larger guests including hydrophobic cationic stimulants **7** and **8** and neutral steroids **10** – **13**. Compounds **10** – **13** were selected to probe the whether a cationic center is required for selectivity with P[6]AS. Additionally, we added beta-blocker labetalol **9** to determine if our sensing assay can differentiate compounds based on their role in the body. Finally, two substances (**1** and **10**) that are not explicitly banned by WADA were selected to demonstrate that our sensing assay can differentiate structurally similar substances that are not banned thereby reducing the chance of type I errors (false-positives). Finally, after some experimentation, we determined that lucigenin and Hoechst 33258 are particularly appropriate dyes to use in concert with P[5]AS and P[6]AS, respectively, to construct indicator displacement assay based sensing ensembles.

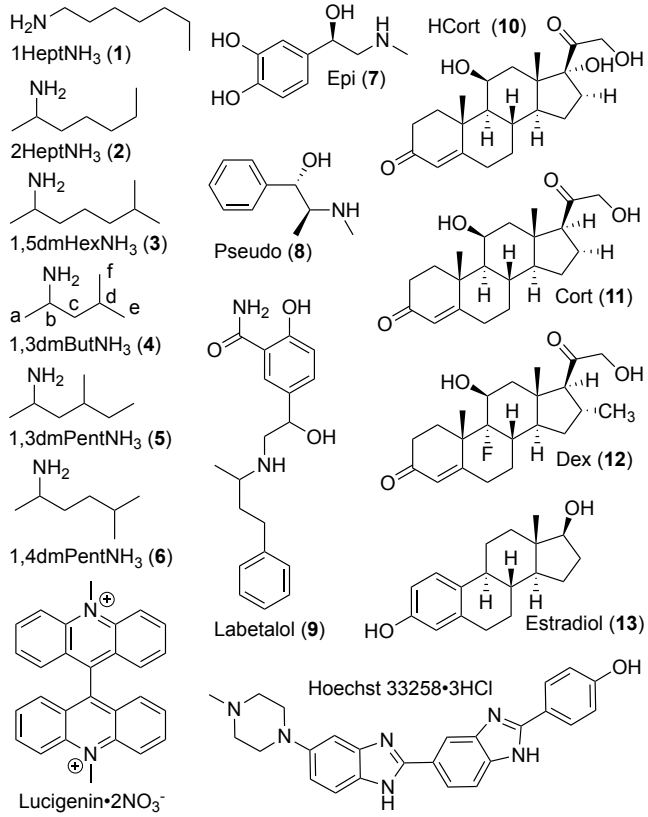

Fig. 2. Chemical structures of WADA banned substances and dyes used in this study.

2.2. Measurement of the thermodynamics of P[n]AS•Guest complexation.

First, we decided to measure the thermodynamics of P[*n*]AS•guest complexation for the WADA-banned substances given in Figure 2. Given the high affinity binding previously reported for P[*n*]AS•guest complexation we elected to employ isothermal titration calorimetry[18] as our primary analytical technique because of its ability to measure K_a values in the 10^3 – 10^7 M^{-1} range by direct ITC titrations.[19] Figure 3a shows a plot of heat evolved versus time during the direct titration of a solution of P[6]AS (25 μM) in the ITC cell with a solution of **2** (250 μM) from the ITC injection syringe. For each ITC titration, the host and guest concentrations were selected to ensure an appropriate Wiseman c-value[18-20] and that full binding isotherm was sampled. The raw heat data in Figure 3a was integrated in order to create the plot of ΔH versus molar ratio shown in Figure 3b which was fitted to a 1:1 binding isotherm using the PEAQ data analysis software to determine the K_a and ΔH values for each run. The titrations were performed in triplicate which gave $K_a = (5.59 \pm 0.32) \times 10^6$ M^{-1} and $\Delta H = -9.17 \pm 0.06$ kcal mol^{-1} for the P[5]AS•**2** complex after error propagation.[21] Analogous direct titrations were performed in triplicate for most of the remaining guests with both P[5]AS and P[6]AS and the results are collected in Table 1.

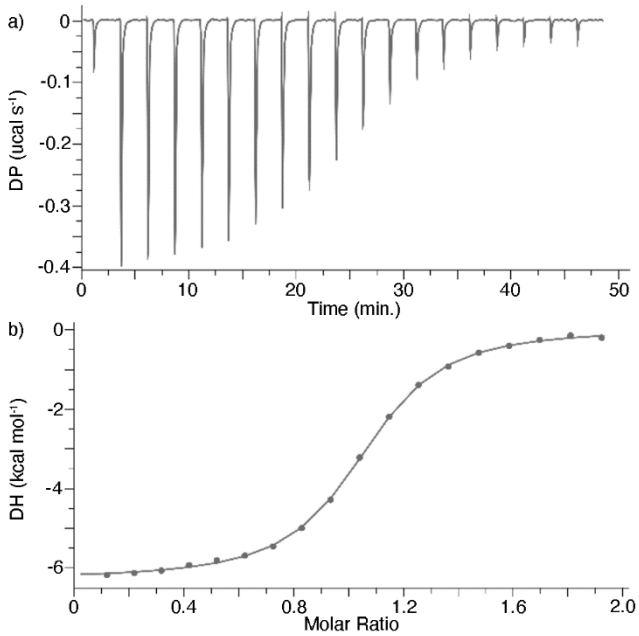

Fig. 3. a) ITC thermogram recorded during the titration of P[6]AS (25.0 μM) in the cell with **2** (250 μM) in the syringe. b) Plot of the integrated heats of each titration *vs.* the molar ratio with the solid line representing the best fit of the data to a 1:1 binding model with $K_a = (5.59 \pm 0.32) \times 10^6$ M^{-1}, $\Delta H = -6.38 \pm 0.03$ kcal mol^{-1}. Conditions: PBS, pH 7.4, 298.0 K.

2.3. Measurement of the binding constants for P[n]AS•dye complexes by fluorescence spectroscopy.

As a prelude to the use of P[*n*]AS•dye complexes as the key components of sensing ensembles for WADA banned substances, we set out to measure the binding affinities for P[5]AS•lucigenin and P[6]AS•Hoechst 33258 by fluorescence spectroscopy. Experimentally, we found that when a PBS solution of lucigenin (4 μM) was titrated with a PBS solution of P[5]AS a quenching of the fluorescence emission at 500 nm (excitation at 365 nm) was observed. Figure S19 shows a plot of fluorescence intensity at 500 nm versus P[5]AS concentration with triplicate measurements at each host concentration which could be fitted to a 1:1 binding model implemented in Scientist™ to determine $K_a = (2.83 \pm 0.14) \times 10^6$ M^{-1} for the P[5]AS•lucigenin complex. In a similar fashion, titration of a PBS solution of Hoechst 33258 (2 μM) with P[6]AS lead to a an ≈ 80-fold increase in fluorescence at 500 nm (excitation 355 nm) followed by a decrease in fluorescence (Figure S20). This biphasic change in fluorescence is not consistent with a simple 1:1 binding model. Hoechst 33258 contains two benzimidazolium binding sites which suggests a 2:1 host:guest binding stoichiometry. Previously, Barooah and co-workers found that CB[7] and CB[8] form 2:1 CB[n]•Hoechst 332582 complexes.[22] Accordingly, we implemented a 2:1 host:guest binding model in Scientist™ which was used to extract $K_{a1:1} = (1.05 \pm 0.36) \times 10^8$ M^{-1} and $K_{a2:1} = (1.27 \pm 0.35) \times 10^6$ M^{-1}.

2.4. Discussion of the trends in P[n]AS•guest binding affinity.

An examination of Table 1 shows that P[5]AS is the more selective host toward **1** – **11** with K_a values from 9650 – 1.1 x 10^7 M^{-1}; ΔH values range from -5.08 to -10.6 kcal mol^{-1}. P[5]AS does not bind to **7**, **8**, **10**, and **11**. P[6]AS displays good affinity across **1** – **11** with K_a values ranging from 2.78 x 10^3 to 6.37 x 10^6 M^{-1}; ΔH values range from -6.38 to -14.1 kcal mol^{-1}. From previous studies,[14] it is known that the pillar[5]arene cavity prefers linear alkyl groups over branched or cyclic alkyl groups. This trend is also seen in the current data set among the four C7-compounds (**1**, **2**, **5**, and **6**) where linear heptylammonium **1** binds 1.9-fold stronger than 2-aminoheptane **2**, 380-fold stronger than branched **5**, and 1130-fold stronger than branched **6**. A comparison of the binding affinity of **4** (6 carbons), **6** (7 carbons), and **3** (8 carbons) which differ by the addition of CH_2-groups between the amino group and the isopropyl terminus is also instructive. A priori, one might expect that the longer and more hydrophobic the guest, the higher the K_a value.[23] Indeed, P[5]AS•**3** is 33-fold weaker than P[5]AS•**4** but P[5]AS•**6** is weaker still. Examination of molecular models (*vide infra*) shows that whereas the isopropyl group of **4** and **6** experience steric interactions with the walls of the narrow P[5]AS host, the isopropyl group of **3** extends out the opposite portal of P[5]AS. The more voluminous P[6]AS host binds all of the guests (**1** – **11)** less selectively with K_a values clustered in the 10^4 – 10^6 M^{-1} range. In this instance the binding affinity of P[6]AS toward **3**, **4**, and **6** follow the expected trend where each additional CH_2-group increases binding affinity. For related reasons, the binding affinity of P[6]AS toward guests **1**, **2**, **5**, and **6** which each contain 7 C-atoms cluster in a very narrow range of 1.82 – 3.65 x 10^6 M^{-1}.

Table 1. Binding Constants measured by ITC for the interaction of P[5]AS and P[6]AS with the panel of WADA-banned substances. Conditions: PBS buffered H_2O, pH 7.40, 298 K.

	P[5]AS		P[6]AS	
Guest	K_a (M^{-1})	ΔH° (kcal mol^{-1})	K_a (M^{-1})	ΔH° (kcal mol^{-1})
1, 1HepNH3 [c]	(1.12 ± 0.06) x 10^7	-6.84 ± 0.03	(3.65 ± 0.22) x 10^6	-7.68 ± 0.07
2, 2HepNH3	(5.59 ± 0.32) x 10^6	-9.17 ± 0.06	(1.82 ± 0.06) x 10^6	-6.38 ± 0.03
3, Octodrine	(1.53 ± 0.08) x 10^6	-9.87 ± 0.08	(6.37 ± 0.43) x 10^6	-7.88 ± 0.05
4, 1,3-dmButNH3	(4.64 ± 0.34) × 10^4	-5.29 ± 0.13	(7.89 ± 0.17) x 10^5	-6.43 ± 0.02
5, 1,3-dmPentNH3	(2.95 ± 0.15) x 10^4	-5.70 ± 0.13	(1.89 ± 0.05) x 10^6	-7.11 ± 0.02
6, 1,4-dmPentNH3	(9.90 ± 0.28) x 10^3	-5.08 ± 0.23	(3.55 ± 0.13) x 10^6	-8.01 ± 0.04
7, Epinephrine	n.b.	n.b.	(4.39 ± 0.17) x 10^4	-9.44 ± 0.14
8, Pseudoephedrine	n.b.	n.b.	(3.76 ± 0.05) x 10^5	-7.94 ± 0.02
9, Labetalol	(9.65 ± 0.27) x 10^3	-10.6 ± 0.1	(9.26 ± 0.13) x 10^5	-11.0 ± 0.0
10, Hydrocortisone	n.b.	n.b.	(2.78 ± 0.18) x 10^4	-12.7 ± 0.4
11, Corticosterone [c]	n.b.	n.b.	(1.84 ± 0.09) x 10^5	-14.1 ± 0.2
Hoechst 33258	–	–	(3.49 ± 1.88) × 10^8 (1:1)	–

			$(1.18 \pm 0.33) \times 10^6$ (2:1)[b]	
Lucigenin	$(2.83 \pm 0.14) \times 10^6$ [a]	–	–	–

a) Measured via change in fluorescence of lucigenin fitted to a 1:1 binding model; b) Measured via change in fluorescence of Hoechst 33258 fitted to a sequential 2:1 (H:G) model; c) Not an explicitly WADA-banned substance; n.b. = no heat detected by ITC; – = not measured.

2.5. Use of ^{1}H NMR spectroscopy to glean information on P[n]AS•guest geometry.

The central cavity of pillar[*n*]arene and related cyclophane hosts are shaped by *n* aromatic rings and therefore constitute a magnetic shielding environment. Accordingly, the changes in guest chemical shift upon P[*n*]AS•guest complexation can be used to deduce the geometry of the complex. For example, Figure 4 shows ^{1}H NMR spectra recorded for mixtures of P[*n*]AS (n = 5 or 6) with (±)-**4**. Figure 4a and 4e show the spectrum of uncomplexed P[5]AS and uncomplexed **4** whereas Figure 4c shows the spectrum of an equimolar mixture which exists as the P[5]AS•**4** complex. Quite interestingly, the resonances for $CH_{3,e}$ and $CH_{3,f}$ of **4** undergo substantial upfield shifts ($\delta\Delta$ = -1.3 and -1.8 ppm) upon formation of the P[5]AS•**4** complex which indicates that these protons are located within the anisotropic magnetically shielding environment defined by the five aromatic walls of P[5]AS. The resonances for H_c and H_d undergo smaller upfield shifts upon complexation ($\delta\Delta$ = -0.4 to -0.6 ppm). Conversely, $CH_{3,a}$ and H_b of **4** undergo only small changes in chemical shift ($\delta\Delta < 0.1$ ppm) upon complexation which indicates that these protons are outside of the cavity of P[5]AS. At a 1:2 P[5]AS:**4** ratio, the resonances for guest **4** shift back toward the chemical shifts of uncomplexed **4** which indicates that the kinetics of guest exchange are fast on the chemical shift timescale. Overall, these results indicate that the tail of **4** is able to enter the cavity of P[5]AS whereas the NH_3^+ head group resides outside the cavity nearby the OSO_3^- groups. Figure 5a shows a cross-eyed stereoview of an energy minimized (MMFF) molecular model of P[5]AS•**4** which is in accord with the geometrical features deduced on the basis of complexation induced changes in chemical shift. Figure 4e and 4i show the ^{1}H NMR spectra recorded for uncomplex **4** and P[6]AS, respectively, whereas Figure 4g shows the ^{1}H NMR spectrum of an equimolar mixture which exists as the P[6]AS•**4** complex. Unlike the observations for P[5]AS•**4**, all of the resonances of guest **4** shift upfield ($\Delta\delta$ from -1.2 to - 2.15 ppm) upon formation of the P[6]AS•**4** complex with largest shifts experienced by $CH_{3,e}$ and $CH_{3,f}$. This observation suggests that the more voluminous P[6]AS is able to more fully encapsulate guest **4** within the anisotropic shielding region of its cavity. Figure 5b shows an MMFF minimized model of P[6]AS•**4**. Figure 4f shows the ^{1}H NMR spectrum recorded for a 1:2 mixture of P[6]AS and **4** which shows the guest resonances shifting back toward the chemical shifts for uncomplexed **4** which establishes fast kinetics of guest exchange on the chemical shift timescale for the P[6]AS•**4** complex. Related sets of ^{1}H NMR spectra were recorded for the complexes between P[*n*]AS (n = 5, 6) with guests 2, 5, and 6 (Figures S21 – S27) which displayed similar patterns of changes in chemical shift upon complexation.

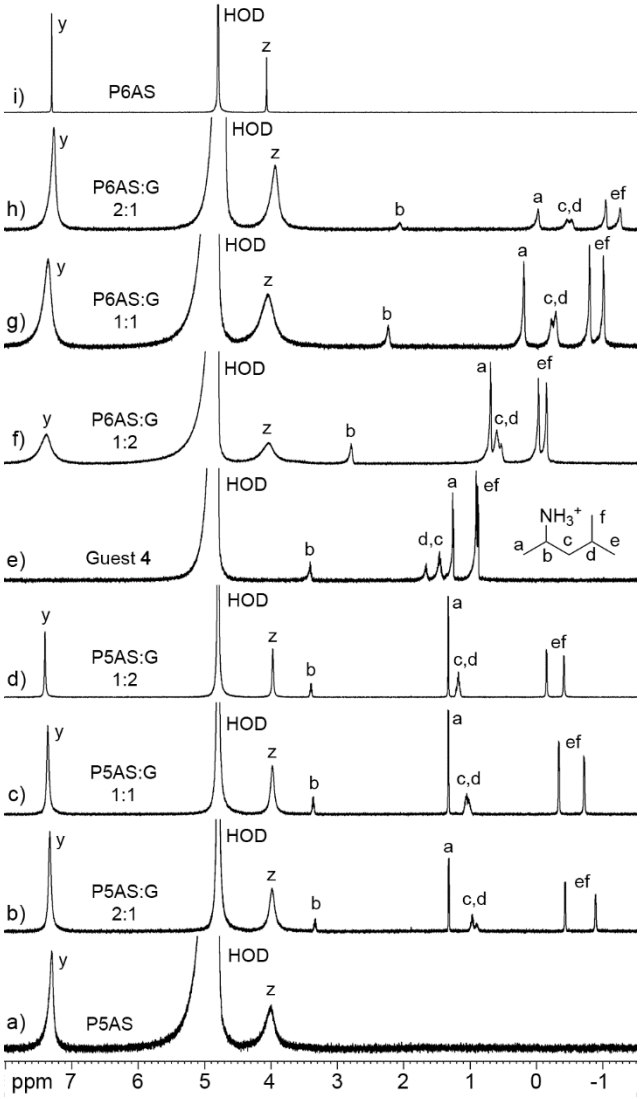

Fig. 4. ^{1}H NMR spectra recorded for (600 MHz, RT, PBS buffered D_2O, pD 7.4) for: a) P[5]AS (1.0 mM), b) a mixture of **4** (0.5 mM) and P[5]AS (1.0 mM), c) an equimolar mixture of **4** and P[5]AS (1.0 mM), and d) a mixture of **4** (2.0 mM) and P[5]AS (1.0 mM), e) **4** (1.0 mM), f) a mixture of **4** (2.0 mM) and P[6]AS (1.0 mM), g) an equimolar mixture of **4** and P[6]AS (1.0 mM), and h) a mixture of **4** (0.5 mM) and P[6]AS (1.0 mM), i) P[6]AS (1.0 mM).

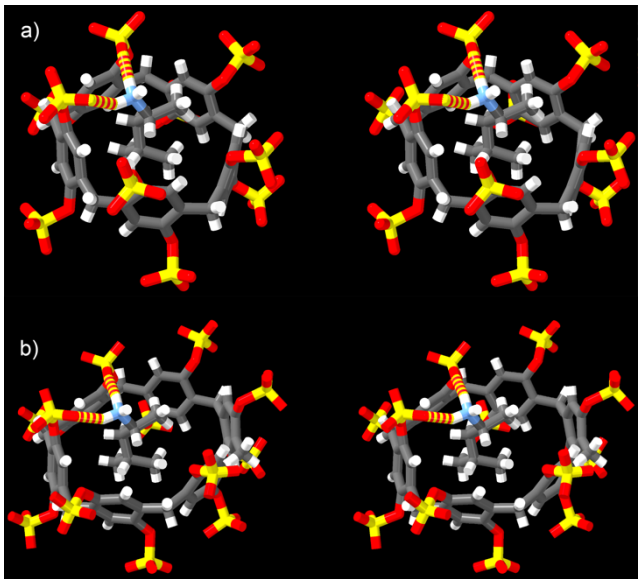

Fig. 5. Cross-eyed stereoviews of MMFF minimized models of: a) P[5]AS•**4** and b) P[6]AS•**4**. Color code: C, grey; H, white; N, blue; O, red; S, yellow; H-bonds, red-yellow striped.

2.6. Detection of WADA Banned Substances in PBS Buffer.

2.6.1. Determination of the conditions for the assay.

In a previous report, we measured the binding constants of P[6]AS toward modified peptides using 4′,6-diamidino-2-phenylindole (DAPI) as the dye to construct and indicator displacement assay.[15b] Initially, we tested the fluorescence response of a series of P[*n*]AS•dye complexes (DAPI, thioflavin T, proflavine, rhodamine 6G, lucigenin, and Hoechst 33258; 2.0 μM concentrations) upon addition of the panel of tighter binding and structurally similar stimulants (**1** – **6**). We found that the largest changes in fluorescence intensity were observed for lucigenin and Hoechst 33258 which was anticipated to result in highest performance in the sensing and differentiation of the WADA-banned substances. Subsequently, we found that assays conducted using P[5]AS•lucigenin and P[6]AS•Hoechst 33258 (2 and 5 μM concentrations) were appropriate; higher concentrations of sensing components were not included during this optimization in order to maximize compound differentiation at low WADA-banned substance concentrations.

2.6.2. Implementation of Linear Discriminant Analysis (LDA) to Detect and Differentiate WADA Banned Substances in PBS Buffer

After identifying appropriate dyes and dye concentrations (P[5]AS•lucigenin at 2 and 5 μM; P[6]AS•Hoechst 33258 at 2 and 5 μM), we turn our attention to determining the best emission wavelengths to monitor. For each condition, the fluorescence emission intensity was measured every 5 nm from 435 – 470 nm (P[5]AS•lucigenin) and from 335 – 435 nm (P[6]AS•Hoechst 33258). Typically, previous researchers have increased the predictive accuracy of related differential sensing assays by working in pure water[24] and at relatively high concentrations of guest in order to maximize the change in spectroscopic signal of the displaced dye.[8] To provide an assessment of the predictive power of this P[*n*]AS-based assay as a method for drug testing, we elected to use the more competitive and biologically relevant PBS buffer (pH 7.4) as our medium. We then determined the lowest concentration of WADA-banned substance that yielded over a 90% accuracy (50 μM) with 15 separate measurements of each analyte.

To prevent overfitting and increase the generality of the sensing protocol, we reduced the number of dimensions (wavelengths) used first by feature selection, then by feature extraction. First, unhelpful and extraneous wavelengths were removed, and the 15 best wavelengths were retained by performing analysis of variance (ANOVA) on the data.[25] To do this, at each wavelength the variance within the repetition measurements for each compound is compared to the total variance of all the signals at that wavelength. This process is then repeated for each wavelength. Wavelengths that have a greater difference between the two different types of variances contain more information and are thus more useful. Three additional wavelengths were added to more effectively detect and differentiate the aromatic guests **7** – **9** and steroids **10** – **14** resulting in a total of 18 variables. From these 18 variables, new variables which explain the data more efficiently, called features or linear discriminants (LD), were found using the feature extraction algorithm linear discriminant analysis (LDA).[25] LDA is a supervised learning technique that finds new variables that are a linear combination of the original variables that both reduce the variance within each class (guest) while maximizing the variance between each class. Figure 6 shows cross plots of the first three linear discriminants. These three discriminants retain 98.5% of the total variance, or information, from the original 18 variables remaining after feature extraction. These LDs not only more efficiently explain the data, but they are also useful for sensing applications because they carefully chosen to reduce the spread within of each group while maximizing the separation between groups.

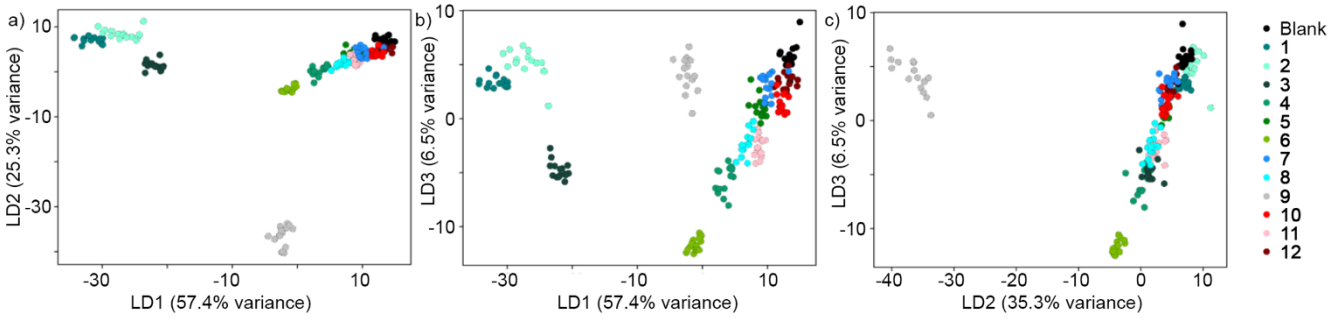

Fig. 6. Cross sections of the three-dimensional LDA plot for the discrimination of 13 WADA-banned compounds at 50 μM of guest. The predictive accuracy was determined to be 92.3 ± 6.9 % as determined via stratified K-fold (K = 15) cross-validation.

LDA can also be used as a predictive tool. To find the predictive power of the assay, stratified K-fold cross validation (CV) with K = 15 was used since there were 15 repetition measurements taken for each compound.[25b] For this purpose, the data from the measurements of the 12 different compounds (guests **1** - **11** and a PBS buffer blank) (50 μM) were randomly separated into 15

different groups such that a single measurement of each compound was randomly assigned to each group. Initially, one of the 15 groups were held-out as the remaining data were used to train an LDA model. After the LDA was trained on the data from the remaining 14 groups, the held-out group was then used to test the accuracy of the model. This was repeated for each of the 15 groups, with a new model trained each time (for a total of 15 models). Using this method, in total, the models were able to predict the held-out data with an average accuracy of 92.3 ± 6.9 %. To more readily see which compounds were the most difficult to accurately predict and which compounds were most often confused for each other, a plot of true compound identity versus the predicted compound identity, known as a confusion matrix, was constructed. If the assay was able to perfectly predict each compound, you would expect to see 15's on the diagonal since the true compound identity and the predicted identity match (Figure S27). For example, Figure S27 shows that **7** was predicted with the lowest accuracy (10/15) and was most often confused for **11**; this makes sense as neither **7** nor **11** bind strongly to P[5]AS and have comparable association constants toward P[6]AS. Because we were satisfied with the predictive accuracy of the model, we did not seek to improve it further by increasing guest concentration, using a less competitive medium, or increasing the number of conditions (e.g. to better differentiate the steroids).

An interesting feature that we recognized was that the LDA plot (Figure 6) separated chemicals of different pharmacological groups. For example, Figure 6c shows that steroids **10** – **12** were separated from the stimulants along a boundary that extends from the blank towards **6**. The LDA function plots the stimulants and steroid data points along the same plane, with only labetalol (**9**, beta-blocker), located in another plane. This suggests that the assay should be able to assign a new unknown analyte to the correct pharmacological group. To test this concept, we measured estradiol **13** – which was not used in creating the classifier – using the same protocol. When the classifier was then asked to predict the identity of the compound, the LDA classifier predicted it was a steroid 80% of the time (**12** – 8 times, **10** – 4 times) and it was twice confused for the blank. This assay offers useful information even when analyzing novel analytes because pharmacologically similar compounds are grouped together.

Since each LD theoretically represents an underlying variable, it is worthwhile to attempt to determine the nature of the underlying variables (LD1 and LD2) because they may shed light on the nature of each binding interaction. It is natural to consider whether LD1 and LD2 correspond to the binding constant of each guest with P[6]AS and P[5]AS. Figures S28 – S31 show plots of each LD versus K_a, log K_a, ΔH, and $-T\Delta S$. Interestingly, the log K_a values (Figure S29) for P[5]AS and P[6]AS show a parabolic correlation with LD1; as LD1 becomes more positive, the K_a for both P[6]AS and P[5]AS trend toward 0.

2.7. Quantitative Detection of Epinephrine and Pseudoephedrine in Simulated Urine.

With the conditions now optimized for the separation of each compound, the ability of the assay to determine concentration in simulated urine was determined. Simulated urine was used as the medium because over 90% of the 241,430 samples tested and entered into the Anti-Doping Administration & Management System (ADAMS) in 2021 were urine samples[26] and to avoid the use of potentially biohazardous human samples. For this purpose, we spike simulated urine with different concentrations of either epinephrine **7** or pseudoephedrine **8** with the goal of accurately detecting them below the competition threshold limits (**7**: 0.27 μM; **8**: 908 μM) defined by WADA.[27] The calibration measurements for concentrations from 0-2500 μM of **8** and 0-100 μM of **7** were collected using the same conditions and wavelengths as above without further optimization. The data was processed with a new LDA algorithm for each analyte to prevent overfitting. The first discriminant was then fitted to a regression support vector machine (rSVM).[25b] A rSVM is similar to traditional linear regression with a few notable exceptions. In this instance, the main advantage of the rSVM is that, instead of fitting a line with infinitely small thickness, it fits a line with a tunable width, ε, on either side of the central line. Any point inside this width is assumed to lie along the line and no penalty is applied to these data points when fitting which reduces the influence of outliers on the fitting. Examination of the data showed that the concentrations of **8** were non-linear with respect to LD1, so the data was transformed into a plot of LD1 *vs.* the natural log of the concentrations. After the line was fit, the concentrations were transformed back to the original space by taking the exponent of the calibrated y values (Figure S32). After calibration, two previously unmeasured concentrations were chosen to test the accuracy of the assay. For **8** one of these two concentrations was between the limit of LOD of our model and the WADA-defined threshold limit, and the other was above the WADA threshold limit. For **7** it quickly became apparent that the current assay would not be able to measure **7** at concentrations close to the WADA-threshold. The results of the calibration and prediction can be seen in Figure 7b. The LOD and LOQ for each model were defined according to previously defined values[25a] of $3\sigma_b$ and $10\sigma_b$ respectively plus the predicted blank concentration, where σ_b represents the standard deviation of the predicted blank concentration.

The calibration plots yielded an LOD of 5.7 μM and LOQ of 19.1 μM for **7** and an LOD of 28.6 μM and LOQ of 31.8 μM for **8**. For **7**, we tested concentrations of 9.3 μM and 41.3 μM and obtained predicted concentrations of 8.6 ± 3.2 μM, and 48.3 ± 4.0 μM, respectively. For **8**, we tested concentrations of 186 μM and 1200 μM, and obtained predicted concentrations of 135.2 ± 7.0 μM and 1270 ± 21 μM, respectively. Unfortunately, the assay is not yet sensitive enough to detect concentrations of **7** near the WADA-threshold. However, the assay can predict the concentration of **8** relatively accurately across a broad range of concentrations. For example, the assay has a LOQ that is 30-fold lower than the WADA threshold while maintaining the ability to predict concentrations above millimolar concentrations with less than 6% error. Taken together, this suggests that this proof-of-concept assay, with further optimization, could be useful as a quick and inexpensive way to screen athletes for banned stimulants.

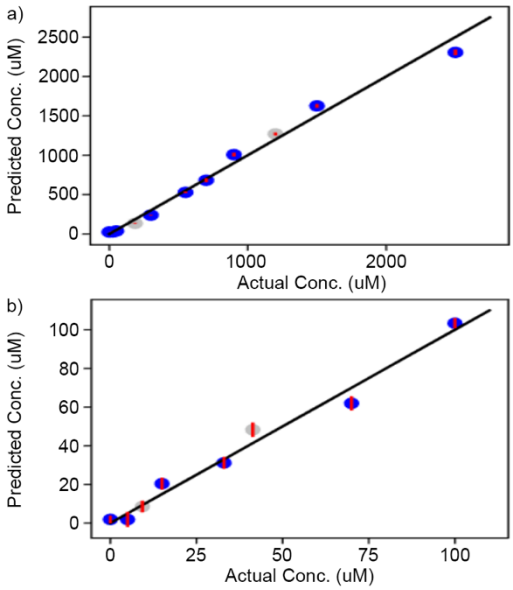

Fig. 7. Calibration plots for ten concentrations were measured (15 replicates per concentration) for: a) **8** from 0 – 2500 μM, and b) **7** from 0 – 100 μM in simulated urine. The calibrations were able to achieve LOD of 85.4 μM and LOQ of 146.8 μM for **8**, and LOD of 5.7 μM and LOQ of 19.1 μM for **7**. The red lines represent the standard deviation of the predicted concentrations. The solid black line represents a perfect correlation between predicted and actual concentrations. Two test concentrations (silver) used for each compound with one above and one below the WADA-LOQ.

3. Conclusions

In summary we have measured the thermodynamics of the binding of P[*n*]AS (n = 5, 6) toward a panel of stimulants, steroids, and a beta-blocker by ITC in PBS buffer. We find that the narrow cavity of P[5]AS selectively binds to alkylammonium ions **1** – **6** relative to the bulkier steroidal and aromatic guests. Binding of branched alkylammoniums (e.g. **5**, **6**) to P[5]AS is disfavored relative to linear alkylammonium **1** due to steric interactions between the Me-branches and the walls of the P[5]AS cavity. Conversely, the larger cavity of P[6]AS binds to the guest panel with a narrow range of binding affinities (27800 – 6.37 x 10^6 M^{-1}). We used ^{1}H NMR spectroscopy to observe the complexation induced changes of guest chemical shift to deduce geometrical features of the P[*n*]AS•guest complexes. P[6]AS with its large cavity can encapsulate the entire hydrophobic regions of the guest resulting in upfield shifting of most resonances whereas P[5]AS is selective for narrow portions of the guest resulting in upfield shifting of a subset of resonances. An indicator displacement assay employing P[*n*]AS (n = 5, 6) and dyes lucigenin and Hoechst 33258 was developed which allowed differentiation of the structurally similar members of the guest panel (50 μM) with over 90 % accuracy in PBS. Although the current assay worked well using spiked artificial urine, additional compounds should be included in the training data if real world samples containing allowed drugs and WADA banned substances are assayed. The assay was further developed to allow the measurement of pseudoephedrine in simulated urine with a LOQ well below the WADA threshold level for drug testing. Overall we have established that P[*n*]AS is a promising class of molecular container containers for the construction of indicator displacement assays and demonstrated their use in a proof-of-concept drug testing assay for a selection of WADA-banned substances.

4. Experimental section

4.1. General information

Chemicals were purchased from commercial suppliers and used without further purification or were prepared by literature procedures.[14-15] Simulated urine was purchased from Flinn Scientific (“Artificial Urine, Normal” Lot#294189). PBS buffer was made by dissolving commercially available tablets (MP Biomedicals, Lot#S7091) in HPLC grade water and adjusting to pH 7.4 using aq. NaOH or HCl. ^{1}H NMR spectra were measured on commercial instruments operating at 600 MHz using sodium phosphate buffered D_2O saline (pD 7.4) as the solvent. Chemical shifts (δ) are referenced relative to the residual resonance for HOD (4.79 ppm). ITC data were collected on a Malvern Microcal PEAQ-ITC instrument and analyzed using the software provided by the vendor. All fluorescence measurements were performed using Greiner Bio-One black, flat-bottomed, polystyrene 96 well plate and measured with a SpectraMax 5e multimode plate reader. Data analysis and machine learning algorithms were implemented in Python using pandas,[28] numPy,[29] and scikit-learn[30] libraries. All data analysis files and csv files for the calibration curves and LDA plot can be found on GitHub: https://github.com/daking11/WADA_sensor.git.

Acknowledgments

We thank the National Science Foundation (CHE-2105857 to L.I.) for financial support.

Supplementary Material

Determination of thermodynamic parameters of binding of P[5]AS and P[6]AS toward guests and dyes by ITC and fluorescence spectroscopy; binding models (1:1 and 2:1) used to analyze the fluorescence titration data; ^{1}H NMR stack plots created for mixtures of P[*n*]AS with selected guests; machine learning data.

References

[1] S. Franjić, J. Phy. Fit Treatment & Sports 8 (2020) 555736.
[2] D. DeIuliis, D. DeIuliis, J. Sport Admin. Supervision 4 (2012) 3-13.
[3] M. Dowling, S. Harris, M. Washington, J. Sport Management 36 (2021) 433-445.
[4] LA28 Initial Sports Programme to be put forward to the IOC Session - Olympic News, https://olympics.com/ioc/news/la28-initial-sports-programme-to-be-put-forward-to-the-ioc-session, Accessed June 15, 2023.
[5] a) S. E. Hadland, S. Levy, Child Adolesc. Psychiatr. Clin. N. Am. 25 (2016) 549; b) E. Marchei, M. A. Ferri, M. Torrens, M. Farré, R. Pacifici, S. Pichini, M. Pellegrini, Int. J. Mol. Sci. 22 (2021) 4000.
[6] M. Raouf, J. J. Bettinger, J. Fudin, Fed Pract. 35 (2018) 38.
[7] a) B. T. Nguyen, E. V. Anslyn, Coord. Chem. Rev. 250 (2006) 3118-3127; b) G. Ghale, W. M. Nau, Acc. Chem. Res. 47 (2014) 2150-2159.
[8] M. A. Beatty, A. J. Selinger, Y. Li, F. Hof, J. Am. Chem. Soc. 141 (2019) 16763-16771.
[9] A. D. Gill, L. Perez, I. N. Q. Salinas, S. R. Byers, Y. Liu, B. L. Hickey, W. Zhong, R. J. Hooley, Chem. Eur. J. 25 (2019) 1740-1745.
[10] E. G. Shcherbakova, B. Zhang, S. Gozem, T. Minami, P. Y. Zavalij, M. Pushina, L. Isaacs, P. Anzenbacher, J. Am. Chem. Soc. 139 (2017) 14954-14960.
[11] a) Y. Jang, M. Jang, H. Kim, S. J. Lee, E. Jin, J. Y. Koo, I.-C. Hwang, Y. Kim, Y. H. Ko, I. Hwang, J. H. Oh, K. Kim, Chem 3 (2017) 641-651; b) E. Biavardi, S. Federici, C. Tudisco, D. Menozzi, C. Massera, A. Sottini, G. G. Condorelli, P. Bergese, E. Dalcanale, Angew. Chem., Int. Ed. 53 (2014) 9183-9188.
[12] S. Stewart, M. Adams Ivy, E. V. Anslyn, Chem. Soc. Rev. 43 (2014) 70-84.

[13] a) S. Sinn, F. Biedermann, Isr. J. Chem. 58 (2018) 357-412; b) J. Chen, R. J. Hooley, W. Zhong, Bioconjugate Chem. 33 (2022) 2245-2253; c) L. You, D. Zha, E. V. Anslyn, Chem. Rev. 115 (2015) 7840-7892; d) H. Zhang, Z. Liu, F. Xin, Y. Zhao, Coord. Chem. Rev. 420 (2020) 213425; e) L. E. Khalil-Cruz, P. Liu, F. Huang, N. M. Khashab, ACS Appl. Mater. Interfaces 13 (2021) 31337-31354; f) Y. Li, J. Wen, J. Li, Z. Wu, W. Li, K. Yang, ACS Sens. 6 (2021) 3882-3897; g) H. Ju, C. N. Zhu, H. Wang, Z. A. Page, Z. L. Wu, J. L. Sessler, F. Huang, Adv. Mater. 34 (2022) 2108163.
[14] W. Xue, P. Y. Zavalij, L. Isaacs, Angew. Chem., Int. Ed. 59 (2020) 13313-13319.
[15] a) A. T. Brockett, W. Xue, D. King, C.-L. Deng, C. Zhai, M. Shuster, S. Rastogi, V. Briken, M. R. Roesch, L. Isaacs, Chem 9 (2023) 881-900; b) D. King, C. R. Wilson, L. Herron, C.-L. Deng, S. Mehdi, P. Tiwary, F. Hof, Org. Biomol. Chem. 20 (2022) 7429-7438.
[16] World Anti-Doping Agency, The Prohibited List, https://www.wada-ama.org/en/prohibited-list, Accessed June 15, 2023.
[17] a) M. Xue, Y. Yang, X. Chi, Z. Zhang, F. Huang, Acc. Chem. Res. 45 (2012) 1294-1308; b) T. Ogoshi, T.-A. Yamagishi, Y. Nakamoto, Chem. Rev. 116 (2016) 7937-8002.
[18] T. Wiseman, S. Williston, J. F. Brandts, L.-N. Lin, Anal. Biochem. 179 (1989) 131-137.
[19] A. Velazquez-Campoy, E. Freire, Nat. Protocols 1 (2006) 186-191.
[20] J. Broecker, C. Vargas, S. Keller, Anal. Biochem. 418 (2011) 307-309.
[21] J. R. Taylor, *An Introduction to Error Anaylsis*, University Science Books, 2nd ed. edn., 1997.
[22] a) N. Barooah, J. Mohanty, H. Pal, A. C. Bhasikuttan, PhysChemChemPhys 13 (2011) 13117-13126; b) N. Barooah, J. Mohanty, A. C. Bhasikuttan, J. Phys. Chem. B 117 (2013) 13595-13603.
[23] a) F. Biedermann, V. D. Uzunova, O. A. Scherman, W. M. Nau, A. De Simone, J. Am. Chem. Soc. 134 (2012) 15318-15323; b) F. Biedermann, W. M. Nau, H.-J. Schneider, Angew. Chem. Int. Ed. 53 (2014) 11158-11171.
[24] a) A. I. Lazar, F. Biedermann, K. R. Mustafina, K. I. Assaf, A. Hennig, W. M. Nau, J. Am. Chem. Soc. 138 (2016) 13022-13029; b) S. Murkli, J. Klemm, D. King, P. Y. Zavalij, L. Isaacs, Chem. Eur. J. 26 (2020) 15249-15258.
[25] a) J. N. Miller, J. C. Miller, *Statistics and Chemometrics for Analytical Chemistry*, Pearson, 6th ed. edn., 2010; b) G. James, D. Witten, T. Hastie, R. Tibshirani, *An Introduction to Statistical Learning*, Springer New York, 2013.
[26] World Anti-Doping Agency, 2021 Anti-Doping Testing Figures, https://www.wada-ama.org/sites/default/files/2023-01/2021_anti-doping_testing_figures_en.pdf, Accessed June 15, 2023.
[27] a) World Anti-Doping Agency, WADA Technical Document-TD2021DL, https://www.wada-ama.org/sites/default/files/resources/files/td2021dl_final_eng_0.pdf, Accessed June 15, 2023; b) World Anti-Doping Agency, WADA Technical Document – TD2022MRPL, https://www.wada-ama.org/sites/default/files/resources/files/td2022mrpl_v1.0_final_eng.pdf, Accessed June 15, 2023.
[28] The pandas development team, pandas-dev/pandas: Pandas, https://zenodo.org/record/7979740, Accessed June 15, 2023, DOI: 10.5281/zenodo.3509134.
[29] C. R. Harris, K. J. Millman, S. J. van der Walt, R. Gommers, P. Virtanen, D. Cournapeau, E. Wieser, J. Taylor, S. Berg, N. J. Smith, R. Kern, M. Picus, S. Hoyer, M. H. van Kerkwijk, M. Brett, A. Haldane, J. F. del Río, M. Wiebe, P. Peterson, P. Gérard-Marchant, K. Sheppard, T. Reddy, W. Weckesser, H. Abbasi, C. Gohlke, T. E. Oliphant, Nature 585 (2020) 357-362.
[30] F. Pedregosa, G. Varoquaux, A. Gramfort, V. Michel, B. Thirion, O. Grisel, M. Blondel, P. Prettenhofer, R. Weiss, J. Vanderplas, A. Passos, D. Cournapeau, M. Brucher, M. Perrot, É. Duchesnay, J. Machine Learning Res. 12 (2011) 2825-2830.